

EPR Spectroscopic Analysis of U7 Hammerhead Ribozyme Dynamics during Metal Ion Induced Folding[†]

Thomas E. Edwards[‡] and Snorri Th. Sigurdsson^{*,‡,§}

Department of Chemistry, University of Washington, Seattle, Washington 98195-1700, and University of Iceland, Science Institute, Dunhaga 3, IS-107, Reykjavik, Iceland

Received March 24, 2005; Revised Manuscript Received July 27, 2005

ABSTRACT: Electron paramagnetic resonance (EPR) spectroscopy was used to examine changes in internal structure and dynamics of the hammerhead ribozyme upon metal ion induced folding, changes in pH, and the presence and absence of ribozyme inhibitors. A nitroxide spin-label was attached to nucleotide U7 of the HH16 catalytic core, and this modified ribozyme was observed to retain catalytic activity. U7 was shown by EPR spectroscopy to be more mobile in the ribozyme–product complex than in either the unfolded ribozyme or the ribozyme–substrate complex. A two-step divalent metal ion dependent folding pathway was observed for the ribozyme–substrate complex with a weak first transition observed at 0.25 mM Mg²⁺ and a strong second transition observed around 10 mM Mg²⁺, in agreement with studies using other biophysical and biochemical techniques. Previously, ribozyme activity was observed in the absence of divalent metal ions and the presence of high concentrations of monovalent metal ions, although the activity was less than that observed in the presence of divalent metal ions. Here, we observed similar dynamics for U7 in the presence of 4 M Na⁺ or Li⁺, which were distinctively different than that observed in the presence of 10 mM Mg²⁺, indicating that U7 of the catalytic core forms a different microenvironment under monovalent versus divalent metal ion conditions. Interestingly, the catalytically efficient microenvironment of U7 was similar to that observed in a solution containing 1 M Na⁺ upon addition of one divalent metal ion per ribozyme. In summary, these results demonstrate that changes in local dynamics, as detected by EPR spectroscopy, can be used to study conformational changes associated with RNA folding and function.

Metal ions facilitate RNA folding and tertiary structure stabilization and have been implemented indirectly and directly in RNA catalysis (1, 2). Interactions of metal ions with the hammerhead ribozyme (Figure 1A), which catalyzes site-specific phosphodiester bond cleavage to process RNA transcripts prepared by rolling circle replication, have been extensively studied by many biochemical and biophysical techniques (3–5). Divalent metal ions appear to be important for catalysis (6, 7), although the ribozyme retains considerable catalytic activity at high ionic strength in the absence of divalent metal ions (8–10). The hammerhead ribozyme was subsequently shown to fold through a two-state metal ion dependent folding pathway as observed by nondenaturing gel electrophoresis (11), FRET¹ measurements (12), isothermal calorimetry (13), and ¹⁹F NMR spectroscopy (14). Crystallographic studies of the hammerhead ribozyme have yielded information about its interaction with metal ions (15–

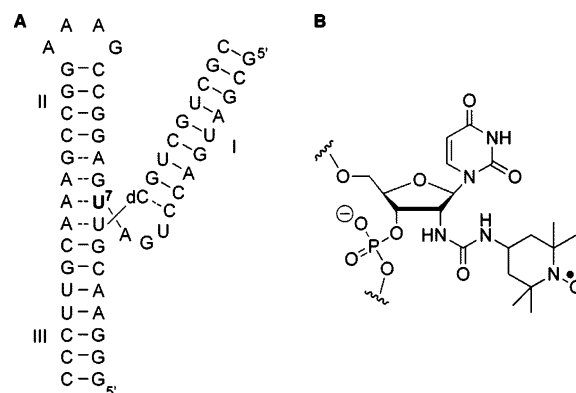


FIGURE 1: (A) The primary and secondary structure of the HH16 hammerhead ribozyme construct. The stems are labeled with roman numerals, and the spin-labeling site is located at U7. A 2'-deoxyribonucleoside (dC) was incorporated at the catalytic site to prevent substrate cleavage during studies of metal ion dependent folding of the ribozyme. (B) Chemical structure of the 2'-spin-labeled uridine nucleotide.

[†] We thank the NIH for financial support (GM56947 and GM62360) and acknowledge a center grant from the National Institutes of Environmental Health Sciences/NIH (GM P30 ES07033) for use of the EPR spectrometer. T.E.E. was supported by a NIH National Research Service Award (5 T32 GM08268).

* To whom correspondence should be addressed. E-mail: snorrisi@hi.is. Tel: +354.525.4801. Fax: +354.552.8911.

[‡] University of Washington.

[§] University of Iceland, Science Institute.

¹ Abbreviations: EPR, electron paramagnetic resonance; cw-EPR, continuous wave EPR; FRET, fluorescence resonance energy transfer; NMR, nuclear magnetic resonance.

17). Although no divalent metal ion binding site was observed proximal to the scissile phosphate, a divalent metal ion binding site was observed at A9/G10.1, approximately 20 Å from the cleavage site. This binding site was shown through a series of biochemical experiments to be the single high-affinity metal ion binding site. For example, replacement of the pro-Rp oxygen of this phosphate with sulfur led to a severe decrease in catalytic efficiency in the presence

of Mg^{2+} ; however, catalytic activity could be subsequently rescued by addition of the thiophilic metal ion Cd^{2+} (10). Although this metal ion binding site appears to be remote from the catalytic site in the ground state, its effect is nonetheless important for catalysis.

Continuous wave (cw) EPR spectroscopy has been used to directly probe metal ion binding to the hammerhead ribozyme (18–21). In these experiments, the commonly studied divalent metal ion, magnesium (Mg^{2+}), is replaced with the paramagnetic metal ion manganese (Mn^{2+}), which allows for the direct study by EPR and can be used to quantify the number of bound divalent metal ions (18, 20, 21). In addition, the pulsed EPR techniques electron spin-echo envelope modulation (ESEEM) spectroscopy (20–22), electron nuclear double resonance (ENDOR) spectroscopy (23), and hyperfine sublevel correlation (HYSCORE) spectroscopy (20, 21) have been used to provide evidence that the single high affinity binding site in solution identified by cw-EPR (18) is likely the A9/G10.1 metal ion binding site observed in all crystal structures.

In addition to obtaining valuable information about binding affinities and the local environment of bound paramagnetic divalent metal ions, it is also possible to apply EPR spectroscopy in conjunction with site-specific nitroxide spin-labeling to the study of global (24) and local (25–35) dynamics in RNA molecules. This paper describes the use of EPR spectroscopy to study changes in the internal structure and dynamics of a hammerhead ribozyme containing a nitroxide spin-label at position U7 (Figure 1) under a variety of experimental conditions including temperature, metal ion identity, ionic strength, and the presence of ribozyme inhibitors. A two-state divalent metal ion dependent folding pathway was observed at low monovalent metal ion concentrations (i.e. low ionic strength), in agreement with other studies. Our results show that U7 exhibited different dynamics in the presence of high concentrations of Na^+ or Li^+ than in the presence of catalytically efficient Mg^{2+} concentrations.

MATERIAL AND METHODS

RNA sample preparation. Unmodified, 2'-deoxy and 2'-amino modified oligoribonucleotides were purchased from Dharmacon, Inc. (Lafayette, CO) and deprotected as described by the manufacturer. Spin-labeled RNA samples were prepared by reaction of 2'-amino modified RNA with 4-isocyanato TEMPO (28) and purified as described (29). Although the spin-labeled RNA used here (38 nucleotides) is longer than those previously employed (less than 20 nucleotides), the spin-labeled RNA was nevertheless resolved from the unlabeled 2'- NH_2 modified RNA by use of a 40 cm tall gel setup and extended electrophoresis times. Literature values of the molar extinction coefficients for the ribozyme strand (HH Rz) and the substrate strand (HH sub) were used (36).

Ion Exchange HPLC. Hammerhead ribozyme catalysis was analyzed by ion exchange HPLC using a Varian ProStar HPLC and a Dynamax DNAPac PA-100 4×250 mm analytical column heated to 50 °C by a Timberline Instruments column warmer. The chromatogram was digitally recorded at 260 nm. A modified procedure from that reported (37) was used and is as follows: solvent A, H_2O ; solvent B, 1.0 M NH_4Cl ; initial conditions, 30% B; linear gradient to

90% over 30 min; return to initial conditions over 3 min. A solution of unmodified HH Rz or U7 2'-spin-labeled HH Rz (0.25 nmol) and cleavable substrate (0.25 nmol) was incubated at 37 °C for 10 min (40 mM MgCl_2 , 4.4 mM NaCl, 4.4 mM Tris·HCl, pH 8.5, 12.5 μL total volume per sample). To denature the sample, 8 M urea (12.5 μL) was added prior to IE HPLC analysis. Ribozyme and substrate strands were identified by comparison of retention times with those of authentic samples.

EPR Spectroscopy. Experimental conditions were selected to be consistent with a report describing the study of hammerhead internal structure by ^{19}F NMR spectroscopy (14). Specifically, for EPR spectroscopy spin-labeled RNA (0.3–1.0 nmol) samples were prepared in 6–20 μL of 10 mM NaCl, 10 mM Tris·HCl, pH 7.5 (50 μM spin-labeled RNA final concentration). Additional metal ion concentrations are described for each experiment but in general were 0–50 mM MgCl_2 , 4 M LiCl, 0.01–4 M NaCl, 50 μM or 10 mM NiCl_2 , 50 μM MnCl_2 or 50–100 μM TbCl_3 . For the pH study, the pH was adjusted to 7.0, 8.0, or 8.5 at room temperature prior to EPR sample preparation. RNA samples, except those used in cleavage time-course experiments, were annealed on a thermal cycler using the following protocol: 90 °C for 2 min, 60 °C for 5 min, 50 °C for 5 min, 40 °C for 5 min, 22 °C for 15 min. Neomycin B (0.5 or 5 mM) was added in 1.0 μL aliquots to the annealed 20 μL RNA sample for the 50 μM and 550 μM neomycin inhibitor binding studies, respectively. While it was not tested for this experiment, we have previously observed that addition of neomycin prior to annealing prevents duplex formation of small RNA duplexes. X-band (9.34 GHz) cw-EPR spectra were digitally recorded on a Bruker EMX spectrometer equipped with a TE102 cavity and a Eurotherm B VT 2000 variable temperature unit between 263.2 and 313.2 K with regulation to ± 0.2 K. Experimental parameters include 3355 G center field, 100 kHz modulation frequency, 1.0 G modulation amplitude, 8 mW power, 20.48 ms time constant, 40.96 ms conversion, 1024 points, 42 s sweep time, 110 G sweep width, typically 50–150 scans for low temperatures (263.2 or 273.2 K) or 12–35 scans for high temperatures (303.2 or 313.2 K). Spin-labeled RNA line samples were prepared in 25 or 75 μL VWR Scientific glass micropipets and stored at 4 °C between experiments. EPR spectral widths ($2A_{zz}$), which span the crest of the low field peak to the trough of the high field peak, were measured directly in WIN-EPR, and the approximate error in these measurements is 0.3 G. EPR spectra were subsequently analyzed using Matlab.

EPR Data Analysis. For fast motion spectra, which have narrow EPR spectral widths ($2A_{zz} < 40$ G, Figure 3), rotational correlation times (τ_R) were calculated as described (24) using eq 1. δ is the centerline width, h_0 is the centerline

$$\tau_R = (6.5 \times 10^{-10}) (\delta) \left(\sqrt{\frac{h_0}{h_{-1}}} - 1 \right) \quad (1)$$

peak amplitude, and h_{-1} is the high field peak amplitude (Figure 3). Rotational correlation times for slow motion spectra ($2A_{zz} > 40$ G) were calculated as described (31, 38) using eq 2. In general, the constants a and b depend on the centerline width (38). Values of 5.4×10^{-10} s and -1.36 , respectively, were used for this study, in which all slow motion spectra had centerline widths of approximately 3 G.

$$\tau_R = a \left(1 - \left(\frac{2A_{zz}}{2A_{zz}^{\max}} \right) \right)^b \quad (2)$$

$2A_{zz}^{\max}$ is the maximum spectral width, which is 75.8 G for this nitroxide. The scaled relative mobility factor, M_s , developed by Hubbell and co-workers as a semiquantitative measure of nitroxide motion, reflects both changes in the nitroxide order parameter (S) and effective correlation time (τ_c) (39). M_s was calculated according to eq 3. δ_i is the

$$M_s = \frac{(\delta^{-1} - \delta_i^{-1})}{(\delta_m^{-1} - \delta_i^{-1})} \quad (3)$$

centerline width of the most immobile spin-probe, and δ_m is the centerline width of the most mobile spin-probe. δ_i and δ_m values reported for the protein spin-label MTSSL (8.4 and 2.1 G, respectively) (39) were used due to a significantly smaller body of literature for RNA (33, 40). M_s is a relative factor, and therefore, the exact choice of δ_i and δ_m does not affect the conclusions. M_s values close to 1 are indicative of relatively high mobility, whereas M_s values close to 0 indicate relatively low mobility.

RESULTS

Effect of Nitroxide Spin-Label on Ribozyme Activity. A nitroxide spin-label was incorporated into the 2'-position of U7 of the hammerhead ribozyme HH16 construct (Figure 1) using known chemistry (28, 29). The effect of this modification on hammerhead ribozyme activity was assayed by performing a single turnover catalysis experiment under conditions similar to those used in the subsequent EPR experiments. The experimental conditions were chosen based on a previous NMR study (14), so that our EPR results would be directly comparable; furthermore, the conditions were amenable to a general cleavage assay developed for ion exchange HPLC analysis (37). The results were analyzed by ion exchange HPLC and compared to results obtained for the unmodified hammerhead ribozyme (Figure 2). After 10 min at 37 °C, the unmodified and the spin-labeled hammerhead ribozyme exhibited a similar extent of cleavage. For example, the uncorrected ratios of the intensities of the cleavage products to ribozyme were 1.0:0.9:5.1 for the unmodified ribozyme and 1.0:1.1:5.0 for the U7 spin-labeled ribozyme; after 3 h, the ratios changed only slightly to 1.0:1.2:3.8 for both ribozymes. Unfortunately, the hammerhead ribozyme strand was indistinguishable from the hammerhead ribozyme-substrate complex in this assay, as determined by comparison of the retention times of the hammerhead ribozyme strand and the ribozyme-noncleavable substrate complex (data not shown). Therefore, the exact catalytic rate could not be determined using this assay. These results, however, in conjunction with the EPR activity assay presented below, demonstrate that the spin-labeled ribozyme was active.

EPR Spectroscopy of Ribozyme-Substrate Complex. EPR spectroscopy can be used to measure the global dynamics of a spin-labeled macromolecule, or in other words, its tumbling in solution. For example, changes in the global dynamics can be used to determine macromolecular complex formation (24). In addition, if conditions are selected to

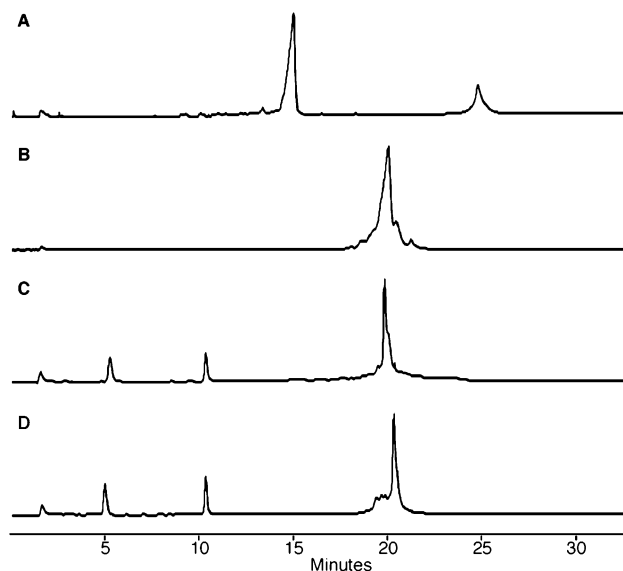


FIGURE 2: HPLC analysis of substrate cleavage by unmodified and U7 2'-spin-labeled hammerhead ribozymes. The peak at ca. 2 min is the column void volume. (A) Analysis of the cleavable substrate (ca. 14.8 min) showed a peak at 25.1 min, which is probably due to the association of two substrate molecules. (B) The unmodified hammerhead ribozyme. (C) Cleavage reaction of the unmodified hammerhead ribozyme (1:1, 0.25 nmol in 12.5 μ L 40 mM MgCl₂, 4.4 mM NaCl, 4.4 mM Tris-HCl, pH 8.5, 20 μ M RNA) after 10 min at 37 °C. The peaks at 5.0 and 10.4 min are the expected cleavage products. (D) Cleavage reaction of U7 2'-spin-labeled hammerhead ribozyme under the conditions described for C.

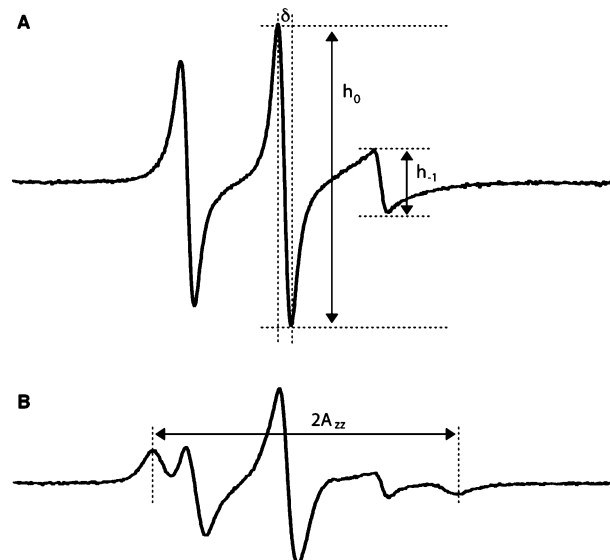


FIGURE 3: EPR spectra of U7 2'-spin-labeled hammerhead ribozyme-noncleavable substrate complex in the absence of divalent metal ions at 40 °C (A) and -10 °C (B), showing a typical fast and slow motion regime EPR spectrum, respectively. EPR spectra of spin-labeled RNA (50 μ M) were recorded in 10 mM NaCl and 10 mM Tris-HCl, pH 7.5. The following spectral features are shown: centerline width, δ ; centerline amplitude, h_0 ; high field line, h_{-1} ; spectral width, $2A_{zz}$.

effectively eliminate macromolecular tumbling on the EPR time scale, internal dynamics or motions can be studied (39). For example, changes in the internal dynamics of a spin-labeled macromolecule can be used to monitor metal ion (29, 31), small molecule (30), or peptide (29, 35) binding. In general, changes in fast motion regime EPR spectra (characterized by narrow EPR spectral width; e.g. $2A_{zz} < 40$ gauss

(G), see Figure 3) may be used to investigate changes in global dynamics such as macromolecular complex assembly, whereas changes in slow motion regime EPR spectra ($2A_{zz} > 40$ G) may be used to monitor changes in local dynamics. The rotational correlation time (τ_R), which is a quantified measurement of nitroxide motion, can be calculated using the centerline width (δ) for fast motion regime spectra (eq 1) or using the EPR spectral width ($2A_{zz}$) for slow motion regime spectra (eq 2) (Figure 3). In general, broader centerline and spectral widths indicate less motion of the probe. By monitoring these changes in dynamics over a range of temperatures, additional information about the macromolecular dynamics may be obtained. In the current study, spectra obtained at higher temperatures (30 to 40 °C) generally exhibited nitroxide mobility in the fast motion regime, whereas spectra obtained at lower temperatures (<20 °C) exhibited nitroxide mobility in the slow motion regime (Figure 3). First, we investigated formation of the ribozyme–substrate complex, and then we investigated the internal dynamics of U7 upon folding.

To study hammerhead ribozyme–substrate complex formation, we used an inhibitory (i.e. noncleavable) substrate with a 2'-deoxy group, which has been previously used to study hammerhead ribozyme–substrate formation (41) and folding (14, 42). At 40 °C in the absence of Mg^{2+} , U7 of the hammerhead ribozyme exhibited motion in the fast regime and had a τ_R of 1.11 ± 0.02 ns, whereas U7 of the hammerhead ribozyme–noncleavable substrate complex had a τ_R of 1.79 ± 0.02 ns (data not shown). Under nonfrozen reduced temperature conditions (−10 °C) in the absence of Mg^{2+} , U7 of the hammerhead ribozyme strand exhibited motion in the slow regime and had a τ_R of 2.59 ± 0.03 ns, whereas in the hammerhead ribozyme–noncleavable substrate complex U7 had a τ_R of 2.89 ± 0.04 ns. These increases in τ_R at a given temperature are consistent with the formation of a larger molecule tumbling more slowly and demonstrate ribozyme–substrate complex formation throughout the temperature range studied here. As an alternative to measuring the rotational correlation time, Hubbell and co-workers developed the relative mobility factor (M_s) as a semiquantitative measure of nitroxide motion (eq 3) (39). Advantages of using the relative mobility factor include the fact that M_s reflects both changes in the nitroxide order parameter (S) and effective correlation time (τ_e) and that M_s can be used throughout both the fast and slow motion regimes. The main disadvantages are that M_s is a relative factor and is therefore only internally comparable and that M_s is calculated based on the centerline width (δ), which makes M_s less sensitive to changes in the slow motion regime where most of our EPR data has been collected. Regardless of these differences, changes in the relative mobility factor M_s were consistent with the changes in τ_R described above. For example, M_s values of 0.54 and 0.97 were observed for the ribozyme strand at −10 and 40 °C, respectively, whereas M_s values of 0.53 and 0.86 were observed for the ribozyme–noncleavable substrate complex at −10 °C and 40 °C, respectively.

For this study, we wanted to monitor changes in the internal dynamics of the hammerhead ribozyme, specifically at U7 of the catalytic core. To determine the extent to which the U7 spin-label reports global or local dynamics, EPR spectra were collected at different viscosities. Addition of

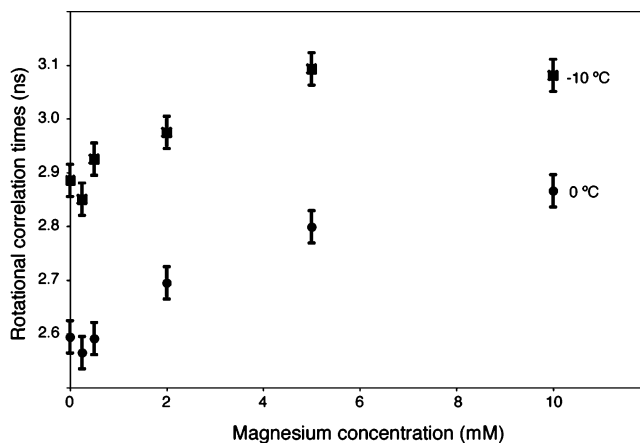


FIGURE 4: EPR spectroscopic analysis of U7 dynamics during Mg^{2+} -induced folding of the hammerhead ribozyme at −10 °C (squares) and 0 °C (circles).

sucrose (14%, w/v) to the solution, which effectively increases the viscosity by 53% at 20 °C (43), had only a minor effect on the EPR spectrum of U7 spin-labeled hammerhead ribozyme–noncleavable substrate complex (data not shown). The addition of sucrose increases the viscosity of the sample without directly interacting with proteins or nucleic acids, unless the sucrose concentration is higher than about 40% (w/v) (24). Our result indicates that the nitroxide spin-label largely reports the local motions of U7 rather than the global motions of the entire ribozyme and implies that the ribozyme is effectively not tumbling on the time scale of the EPR experiments. This result is not surprising given the relatively large size of the RNA complex (55 nucleotides, ca. 17.8 kDa). Consequently, addition of sucrose was not necessary to slow the global tumbling of the molecule in subsequent EPR experiments, as was the case for previous studies of internal dynamics of smaller RNA complexes (e.g. the 27 nt TAR RNA, ca. 9 kDa) (28–31, 35).

Mg²⁺-Induced Hammerhead Ribozyme Folding. To monitor the magnesium-dependence of the hammerhead ribozyme folding pathway, U7 spin-labeled ribozyme samples were incubated over a range of Mg^{2+} concentration (0, 0.25, 0.5, 2, 5, 10, 50 mM) and temperatures (−10, 0, 10, 20, 30, 40 °C). At all temperatures, except 30 °C and 40 °C, the EPR spectral width ($2A_{zz}$) of U7 decreased slightly in the presence of 0.25 mM Mg^{2+} , before increasing in the presence of higher Mg^{2+} concentrations; the latter effect reached a plateau from 10 mM to 50 mM, and higher Mg^{2+} concentrations were not investigated. Although the effect is small and the error bars for these data points overlap, the first transition at lower Mg^{2+} concentrations is clearly visible at lower temperatures (−10 and 0 °C), as demonstrated by changes in the rotational correlation time (Figure 4). The second transition exhibits larger changes in the EPR spectral width and is clear at all temperatures. These EPR results indicate that the first folding event occurs around 0.25 mM Mg^{2+} , while the second folding event is completed at ca. 10 mM Mg^{2+} .

Monitoring Ribozyme Cleavage by EPR Spectroscopy. The conditions investigated above, which demonstrated ribozyme–substrate complex formation and folding, were employed in a single turnover catalysis assay designed to monitor the mobility of U7 by EPR spectroscopy during hammerhead ribozyme cleavage. The solution was cooled to 0 °C to slow

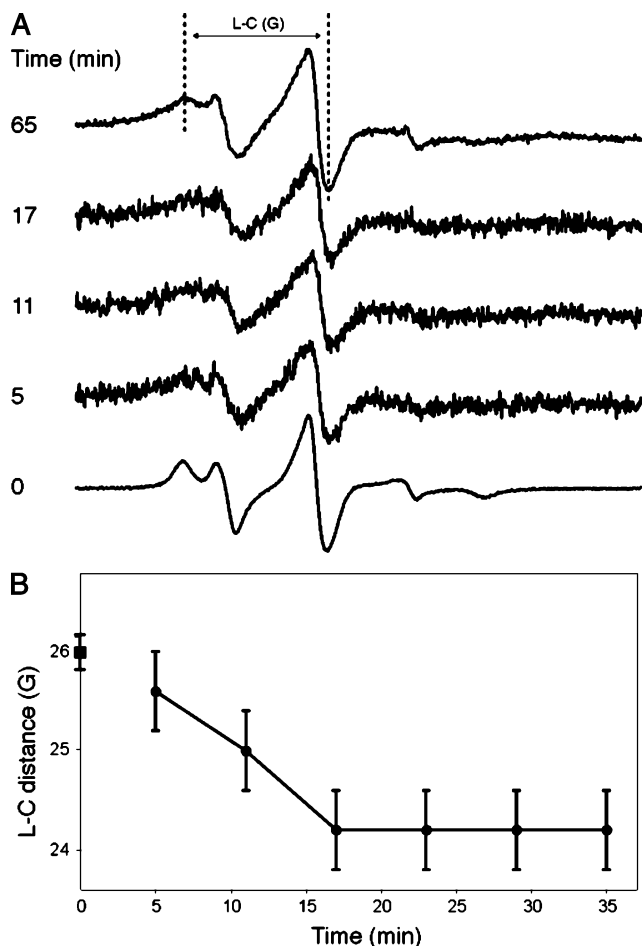


FIGURE 5: (A) Changes in the EPR spectrum were monitored during cleavage of the hammerhead ribozyme. While enough signal intensity could not be attained to measure $2A_{zz}$ due to rapid cleavage, the distances from the low field peak to the trough of the center line were measured (the L-C distance) and plotted (B).

the cleavage reaction and allow for the accumulation of EPR data. Because only a few scans could be acquired for each data point along the time course, strong enough signal intensity could not be accumulated to clearly define the high field peak, and consequently, an accurate measurement of $2A_{zz}$ could not be obtained (for comparison, each scan takes 42 s and complete cleavage is expected after about 10 min at 25 or 37 °C). However, the distance between the crest of the low field peak and the trough of the centerline peak could be measured. This distance decreased linearly over about 18 min starting from the expected distance measured using the noncleavable substrate under the above conditions, and did not change after further incubation, indicating that the reaction was complete (Figure 5). τ_R effectively increased from 2.76 ± 0.04 ns prior to cleavage to 2.54 ± 0.03 ns after cleavage. This τ_R value is slightly faster than that of the unfolded ribozyme–substrate complex in the absence of Mg^{2+} (2.59 ± 0.03 ns) and of the ribozyme in the absence of substrate and presence of Mg^{2+} (2.70 ± 0.03 ns). The latter is the expected state if the products have been released; however, the HH16 construct employed here was designed to effectively not release the products (41). These results demonstrate that EPR could be used to monitor the cleavage event and that U7 was more mobile in the cleaved state.

Monovalent Metal Ion Induced Hammerhead Ribozyme Folding. The hammerhead ribozyme has been shown to be

active in the absence of divalent metal ions and the presence of high concentrations of monovalent metal ions, prompting the hypothesis that the metal ions are not directly involved in catalysis but, rather, are simple structural supports (8). Therefore, we decided to use EPR spectroscopy to investigate U7 dynamics in the presence of high concentrations of monovalent metal ions in comparison with results obtained in the presence of divalent metal ions. The presence of high concentrations of monovalent metal ions alters the natural viscosity of the EPR sample, and therefore, direct comparison of monovalent and divalent metal ion data at a given temperature may not reflect comparative mobilities. For example, the viscosity of 4 M NaCl is ca. 1.53 cP at 20 °C whereas the viscosity of water is 1.00 cP at 20 °C (43). The viscosity of 4 M LiCl was assumed to be close to that of 4 M NaCl. For the magnesium-containing sample, the percent mass composition of salts (10 mM $MgCl_2$, 10 mM NaCl, 10 mM Tris·HCl, pH 7.5) is <0.3% (w/v) and has a negligible effect on the viscosity; thus the reported viscosity of water was used for these solutions. To compensate for the higher viscosity of the 4 M Li^+ or Na^+ solutions, 14% sucrose (w/v) was added to the solution containing the catalytically efficient Mg^{2+} concentration (10 mM) to give this solution a viscosity of 1.53 cP at 20 °C (43). EPR spectra were obtained for each of these solutions over a range of temperatures (Figure 6). The spectra obtained for the Li^+ and Na^+ samples were quite similar. In contrast, U7 had a wider spectral width in the presence of monovalent metal ions than in the presence of Mg^{2+} at all temperatures. The difference in the EPR spectral width in the presence of 10 mM Mg^{2+} compared to 4 M Li^+ or 4 M Na^+ was most pronounced above 20 °C. These results show that the mobility of U7 is higher in the presence of divalent metal ions than under conditions of high concentration of monovalent metal ions.

Possible Structure and Dynamics Recovery with One Divalent Metal Ion per Ribozyme. DeRose and co-workers have shown using cw-EPR spectroscopy that the number of bound divalent metal ions depends on the concentration of monovalent metal ions (18). For example, in the presence of 1.0 M NaCl at low divalent metal ion concentration, one Mn^{2+} was bound with an apparent $K_d \sim 4 \mu M$. In these experiments, it is assumed that Mn^{2+} binds in a similar manner as Mg^{2+} , which is supported indirectly by comparable catalytic rates (6). Because of the observed differences in U7 mobility in the presence of catalytically efficient Mg^{2+} concentrations and in the presence of high concentrations of monovalent metal ions, we decided to test if the U7 dynamics observed in the presence of 10 mM Mg^{2+} could be recovered by addition of one equivalent of divalent metal ions to a solution containing a high concentration (1 M) of monovalent metal ions. The results are shown in Figure 7, which compares the U7 EPR spectral width in the presence of either 10 mM Mg^{2+} or 1.0 M Na^+ in the presence of 50 μM Mg^{2+} . These results indicate similar conformational dynamics for catalytically efficient magnesium concentrations (10 mM) as in the presence of one equivalent of magnesium and high sodium concentrations. Mn^{2+} (Figure 8) or Ni^{2+} (data not shown) could substitute for Mg^{2+} in this experiment and produced nitroxide spectra similar to that obtained for Mg^{2+} . For the Mn^{2+} replacement spectra, increasing intensity of the Mn^{2+} signal was observed as the temperature increased

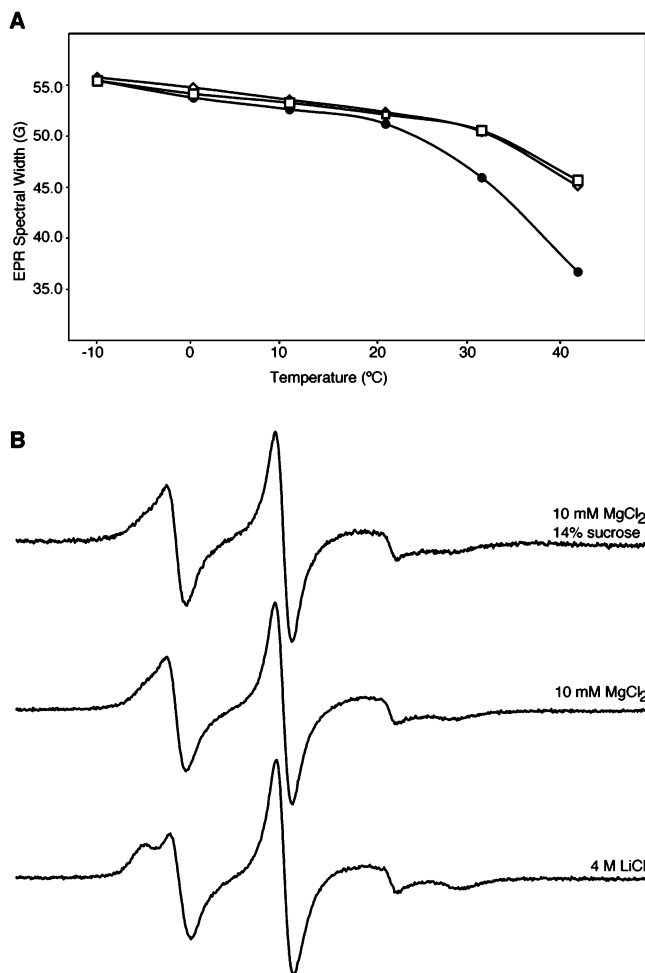


FIGURE 6: (A) Comparison of U7 hammerhead ribozyme dynamics in the presence of 4 M Li⁺ (open diamonds), 4 M Na⁺ (open squares), and 10 mM Mg²⁺/14% sucrose (w/v) (closed circles). Error bars are similar in size to the data point markers. (B) EPR spectra of the hammerhead ribozyme at 30 °C in the presence of 10 mM Mg²⁺/14% sucrose (w/v) (top), 10 mM Mg²⁺ (middle), and 4 M Li⁺ (bottom).

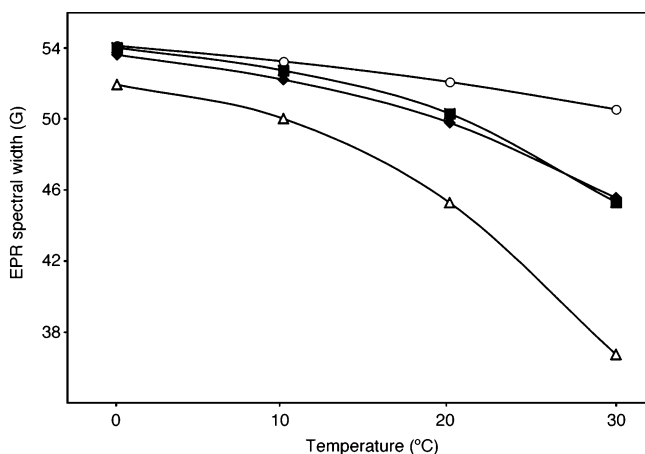


FIGURE 7: Changes in U7 dynamics as a function of temperature in the presence of 10 mM Mg²⁺ (closed diamonds), 1.0 M NaCl, 50 μM Mg²⁺ (1.0 equiv) (closed squares), 4 M NaCl (open circles), and background buffer (10 mM NaCl and 10 mM Tris•HCl, pH 7.5, open triangles). RNA concentration was 50 μM. Error bars are approximately two-thirds the size of the data point markers.

(Figure 8). Bound Mn²⁺ ions do not exhibit an EPR signal at X-band frequencies due to an increase in the zero-field splitting which leads to degenerate energy levels (18),

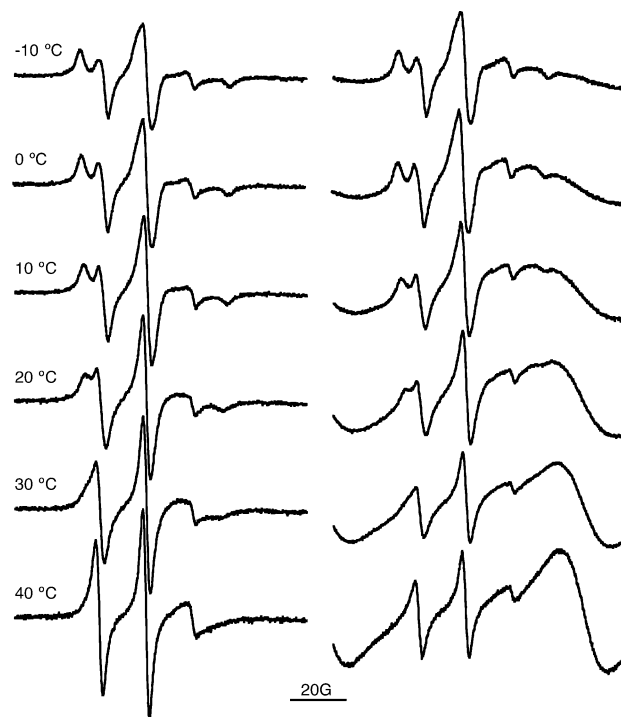


FIGURE 8: EPR spectra of U7 spin-labeled hammerhead ribozyme–noncleavable substrate complex (50 μM) in the presence of 1.0 M NaCl and either 50 μM MgCl₂ (left column) or 50 μM MnCl₂ (right column). Spectra were recorded in 10 mM Tris•HCl, pH 7.5.

whereas unbound Mn²⁺ ions exhibit an EPR signal. These results demonstrate that, under conditions employed to generate a single bound divalent metal ion, Mn²⁺ can replace Mg²⁺ while producing similar U7 mobility and, furthermore, that the divalent metal ion releases from the ribozyme as the temperature is increased.

pH Dependence of U7 Dynamics. A pH-dependent conformational change at pH 8.5 has been proposed to be necessary prior to catalysis (17). Therefore, we monitored U7 dynamics in the presence of catalytically efficient Mg²⁺ concentrations (10 mM) over a range of pH (7.0, 7.5, 8.0, and 8.5). Over a range of temperatures, the spectral width of U7 reached a maximum between 7.5 and 8.0, indicating a slight but distinct decrease in dynamics at this pH (data not shown).

Effects of Ribozyme Inhibitors on U7 Dynamics. Tb³⁺ (44, 45) and neomycin (20, 46–49) are known to bind to the hammerhead ribozyme and inhibit phosphodiester bond cleavage. Tb³⁺ binds to N3 on the base-pairing face of G5 through outer sphere coordination with a $K_d \sim 5 \mu\text{M}$ and to other sites on the hammerhead ribozyme with considerably weaker affinity (45). We studied the dynamics of U7 in the presence of 50 and 100 μM Tb³⁺, but observed only subtle changes in RNA internal dynamics (data not shown). This result is in agreement with the crystal structure obtained in the presence of Tb³⁺, which displayed virtually no change in RNA global or local conformation upon Tb³⁺ binding (44). The aminoglycoside antibiotic neomycin inhibits hammerhead ribozyme cleavage with a K_i of 13.5 μM (47) and, therefore, should be specifically bound at 50 μM neomycin concentrations. Essentially no changes in U7 dynamics were observed in the presence of 50 μM neomycin (1 equivalent to RNA as used in this experiment). At higher neomycin concentrations (550 μM) a decrease in U7 dynamics was

observed (data not shown). In addition to the observed widening of the EPR spectral width, the spectral features were broadened, indicating that numerous bound states likely existed in solution at high neomycin concentrations; these results imply that nonspecific neomycin–ribozyme interactions were observed at the higher neomycin concentrations.

DISCUSSION

Although the hammerhead ribozyme has been extensively studied by many biochemical and biophysical techniques (3–5, 50), a complete picture of the active structure including the role of metal ions has not emerged. Interestingly, certain elements of the hammerhead ribozyme structure were lost for a period of time due to the development of the “minimal” trans-cleaving hammerhead ribozyme construct (51). Specifically, an interaction between loops at the end of stem I and within stem II was discovered recently to affect the catalytic rate (52, 53), folding properties (54), and metal ion requirements (21, 54). Although this interaction is clearly important for the global structure of the cis-cleaving hammerhead, we decided to further investigate the structure and dynamics of the well-characterized HH16 trans-cleaving hammerhead as a means of comparison with the large body of data available on this “minimal” hammerhead ribozyme construct. Here, we use EPR spectroscopy to investigate changes in the internal structure and dynamics of the hammerhead ribozyme, specifically at U7, upon folding under a variety of environmental conditions. This report is significant in that the bulk of the available literature on the hammerhead ribozyme has focused on examining the global structure, whereas only a few techniques have been able to measure internal changes in structure and/or dynamics upon folding (e.g. fluorescence correlation spectroscopy with 2-aminopurine (14, 42, 48, 55) and ^{19}F NMR with 5-fluorouridine (14)). Therefore, one of the goals of this work was to demonstrate the capacity of EPR spectroscopy to study conformational changes and folding in functionally interesting RNA molecules.

U7 was selected as the site for spin-label incorporation because it is located near the catalytic core and, therefore, should be an indicator of structural changes that involve the catalytic core. U7 has been shown to tolerate mutations such as 2-aminopurine (42), and substitution with a 2'-(3-mercapto)-propionamido group only reduced the catalytic efficiency by ca. 10% (56). Furthermore, U7 has been previously labeled in fluorescence correlation spectroscopy (42) and ^{19}F NMR spectroscopy (14) studies, and thus provides an avenue for comparison with previous results. For the current study, a nitroxide spin-label was site-specifically incorporated at U7 by coupling an isocyanate-derivatized nitroxide with U7 2'-amino-modified RNA using previously described chemistry (28) and purification methods (29). Previously, we showed that spin-labels have only a minor effect on RNA stability (28) and RNA-protein binding (29). Nevertheless, it was necessary to establish whether the spin-labeled ribozyme was fully active, and thus a single turnover experiment was carried out under the conditions of the EPR experiment. HPLC analysis of the reaction revealed that the U7 spin-labeled hammerhead ribozyme was catalytically active (Figure 2). Although the exact rate was not determined for the spin-labeled ribozyme, we estimate that the catalytic rate for the spin-labeled sample is at least 0.07 min^{-1} . This rate represents a ca. 10^5 -fold activation over the

uncatalyzed reaction, and it is likely that the exact rate is closer to the HH16 literature value of 1 min^{-1} (41). Furthermore, we were able to monitor the cleavage event by observing a change in the U7 EPR spectrum of the ribozyme–cleavable substrate complex, which indicated rapid cleavage, even at 0°C . U7 was more mobile in the ribozyme–product complex than in the ribozyme–substrate complex. This observation is supported by previous NMR data that showed a significant structural rearrangement in the ribozyme after cleavage (57) and indirectly by the observation that crystals of the hammerhead ribozyme rapidly degrade upon cleavage (58), presumably due to a loss of order in the crystal.

In the current study we observed changes in the EPR spectral width of a U7 nitroxide spin-labeled hammerhead ribozyme, which indicate changes in mobility over a variety of temperatures and ionic conditions. In general, the EPR spectral widths changed up to 3 G at the lower temperatures (-10 to 10°C). These changes were smaller than those observed for the trans activation responsive region (TAR) RNA of HIV at low temperatures (0°C) in the presence of metal ions (up to 11 G), small molecules (up to 8 G), or peptides derived from the Tat protein (up to 20 G). Although the changes observed here were often subtle, the strength of this approach is the patterns that emerged over a range of temperatures. These patterns allowed us to derive information about the structural dynamics of the hammerhead ribozyme during metal ion induced folding and catalysis, which is significant given the lack of information on the structural changes in the catalytic core during hammerhead ribozyme folding and catalysis. Furthermore, these relatively subtle changes may be indicative of a relatively flexible nature of the hammerhead ribozyme and/or the minimal HH16 construct, which lacks the loop–loop interaction found in native hammerhead ribozyme (52, 53).

The folding pathway was investigated by monitoring the changes in the EPR spectrum of U7 in a ribozyme bound to a noncleavable substrate upon incubation with a range of magnesium concentrations. The EPR results appear to indicate a two-step folding pathway with the first folding event around 0.25 mM Mg^{2+} and the second around 10 mM Mg^{2+} (Figure 4), consistent with data obtained by comparative nondenaturing gel electrophoresis (11), FRET measurements (12), isothermal titration calorimetry (13), and ^{19}F NMR spectroscopy (14). In comparison, either a one- or two-step folding pathway was observed using fluorescence correlation spectroscopy, depending on the position of the 2-aminopurine fluorophore (42). These results are presented with the caveat that the error bars at the low Mg^{2+} samples overlap and thus this effect is within statistical noise. Nevertheless, this small increase in U7 dynamics at 0.25 mM Mg^{2+} appears at all temperatures below 30°C . Furthermore, a small change in U7 is consistent with data obtained by ^{19}F NMR, which revealed a change in chemical shift of 0.1 ppm at low Mg^{2+} concentrations. These results indicate that the catalytic core undergoes minor changes during the first transition, but more extensive changes during the second structural transition. However, it is possible that nucleotides other than U7 in the catalytic core may undergo larger changes during the first transition.

It has been observed that the hammerhead ribozyme is active in the absence of divalent metal ions and in the

presence of high concentrations of monovalent metal ions (8–10), leading one to ponder the importance of metal ions on structure and catalysis of the ribozyme (2). Lithium (Li^+) has the highest reported monovalent metal ion catalytic rate, while sodium (Na^+) is substantially lower (9) and ammonium (NH_4^+) is even lower; still, none of these are within 100-fold of the catalytic rate obtained in the presence of Mg^{2+} under similar experimental conditions (59). Mutations within the catalytic core of the hammerhead ribozyme produce similar effects on the catalytic rate observed in the presence of either Li^+ or Mg^{2+} , with the possible exception of mutation at either G10.1 or C11.1. One possible interpretation is that the catalytic mechanism might be the same under monovalent or divalent metal ion conditions with the caveat that a metal ion specifically bound to A9/G10.1 might provide a slight stimulatory effect (10). Using EPR spectroscopy, we show here that monovalent metal ions Li^+ and Na^+ produce similar U7 conformation dynamics, assuming that the viscosities of the 4 M Na^+ and 4 M Li^+ solutions are similar. However, under similar viscous conditions, the Mg^{2+} produced different U7 dynamics, indicating that the monovalent metal ions produce a different U7 microenvironment in comparison with Mg^{2+} . This observation could be due to the absence of a divalent metal ion specifically bound at A9/G10.1.

Interestingly, the conformational dynamics obtained in the presence of catalytically efficient concentrations of Mg^{2+} were similar to those observed in 1 M monovalent metal ions upon the addition of a single equivalent of a divalent metal ion (Figure 7). The fact that Mn^{2+} produced virtually identical U7 conformational dynamics as obtained for Mg^{2+} provides strong evidence that these two metal ions bind in the same manner under these conditions (Figure 8). This is the first report to provide dynamic information (and thus structural information by inference) that Mg^{2+} and Mn^{2+} bind similarly under single divalent metal ion binding conditions (i.e. in the presence of 1 M Na^+ and only 1 equivalent of divalent metal ions). Under conditions similar to our EPR experiments, cw- and pulsed EPR data indicated the presence of a single high affinity Mn^{2+} -binding site (18, 20, 21) consistent with binding to the A9/G10.1 site (20–23) that had been observed in the crystal structure (16). Previously, a similar type of rescue experiment was performed in the presence of high concentrations of divalent metal ion (10 mM M^{2+}) and monovalent metal ions (4 M M^+) (10); however, conditions were not chosen in which a single divalent metal ion was coordinated to A9/G10.1, and thus it was unclear whether or not the rescue effect was directly due to divalent metal ion coordination at this site.

In summary, we have used EPR spectroscopy to investigate metal ion induced folding in the hammerhead ribozyme as well as the effect of pH and the presence of two known inhibitors. This spectroscopic technique enabled us to observe the previously described two-step metal ion induced folding of the ribozyme–substrate complex. Our results demonstrate that different U7 dynamics are observed in the presence of catalytically efficient divalent metal ion concentrations than in the presence of high concentrations of monovalent metal ions. Furthermore, similar dynamics of U7 were observed for the catalytically efficient conditions and high concentrations of monovalent metal ions containing one equivalent of a divalent metal ion, which binds to the single high-affinity

binding site at A9/G10.1. The results presented in this paper demonstrate the ability of EPR spectroscopy to investigate internal changes in ribozyme structure and dynamics in folding and function and show how the study of internal dynamics can yield information about conformational changes.

ACKNOWLEDGMENT

We thank B. H. Robinson for many helpful discussions, D. Herschlag for valuable suggestions and insightful comments, and the Sigurdsson research group for critical reading of this manuscript.

REFERENCES

1. Fedor, M. J. (2002) The role of metal ions in RNA catalysis, *Curr. Opin. Struct. Biol.* 12, 289–295.
2. DeRose, V. J. (2003) Metal ion binding to catalytic RNA molecules, *Curr. Opin. Struct. Biol.* 13, 317–324.
3. Sigurdsson, S. Th., Thomson, J. B., and Eckstein, F. (1998) Small ribozymes, in *RNA Structure and Function* (Simmons, R. W., and Grunberg-Manago, M., Eds.), pp 339–376, Cold Spring Harbor Laboratory Press, Woodbury, NY.
4. Hammann, C., and Lilley, D. M. (2002) Folding and activity of the hammerhead ribozyme, *ChemBioChem* 3, 690–700.
5. DeRose, V. J. (2002) Two decades of RNA catalysis, *Chem. Biol.* 9, 961–969.
6. Dahm, S. C., and Uhlenbeck, O. C. (1991) Role of divalent metal ions in the hammerhead RNA cleavage reaction, *Biochemistry* 30, 9464–9469.
7. Dahm, S. C., Derrick, W. B., and Uhlenbeck, O. C. (1993) Evidence for the role of solvated metal hydroxide in the hammerhead cleavage mechanism, *Biochemistry* 32, 13040–13045.
8. Murray, J. B., Seyhan, A. A., Walter, N. G., Burke, J. M., and Scott, W. G. (1998) The hammerhead, hairpin and VS ribozymes are catalytically proficient in monovalent cations alone, *Chem. Biol.* 5, 587–595.
9. Curtis, E. A., and Bartel, D. P. (2001) The hammerhead cleavage reaction in monovalent cations, *RNA* 7, 546–552.
10. O'Rear, J. L., Wang, S., Feig, A. L., Beigelman, L., Uhlenbeck, O. C., and Herschlag, D. (2001) Comparison of the hammerhead cleavage reactions stimulated by monovalent and divalent cations, *RNA* 7, 537–545.
11. Bassi, G. S., Mollegaard, N. E., Murchie, A. I., von Kitzing, E., and Lilley, D. M. (1995) Ionic interactions and the global conformations of the hammerhead ribozyme, *Nat. Struct. Biol.* 2, 45–55.
12. Bassi, G. S., Murchie, A. I., Walter, F., Clegg, R. M., and Lilley, D. M. (1997) Ion-induced folding of the hammerhead ribozyme: a fluorescence resonance energy transfer study, *EMBO J.* 16, 7481–7489.
13. Hammann, C., Cooper, A., and Lilley, D. M. (2001) Thermodynamics of ion-induced RNA folding in the hammerhead ribozyme: an isothermal titration calorimetric study, *Biochemistry* 40, 1423–1429.
14. Hammann, C., Norman, D. G., and Lilley, D. M. (2001) Dissection of the ion-induced folding of the hammerhead ribozyme using ^{19}F NMR, *Proc. Natl. Acad. Sci. U.S.A.* 98, 5503–5508.
15. Pley, H. W., Flaherty, K. M., and McKay, D. B. (1994) Three-dimensional structure of a hammerhead ribozyme, *Nature* 372, 68–74.
16. Scott, W. G., Finch, J. T., and Klug, A. (1995) The crystal structure of an all-RNA hammerhead ribozyme: a proposed mechanism for RNA catalytic cleavage, *Cell* 81, 991–1002.
17. Murray, J. B., Dunham, C. M., and Scott, W. G. (2002) A pH-dependent conformational change, rather than the chemical step, appears to be rate-limiting in the hammerhead ribozyme cleavage reaction, *J. Mol. Biol.* 315, 121–130.
18. Horton, T. E., Clardy, D. R., and DeRose, V. J. (1998) Electron paramagnetic resonance spectroscopic measurement of Mn^{2+} binding affinities to the hammerhead ribozyme and correlation with cleavage activity, *Biochemistry* 37, 18094–18101.
19. Hunsicker, L. M., and DeRose, V. J. (2000) Activities and relative affinities of divalent metals in unmodified and phosphorothioate-substituted hammerhead ribozymes, *J. Inorg. Biochem.* 80, 271–281.

20. Schiemann, O., Fritscher, J., Kisseleva, N., Sigurdsson, S. Th., and Prisner, T. F. (2003) Structural investigation of a high-affinity MnII binding site in the hammerhead ribozyme by EPR spectroscopy and DFT calculations. Effects of neomycin B on metal-ion binding, *ChemBioChem* 4, 1057–1065.
21. Kisseleva, N., Khvorova, A., Westhof, E., and Schiemann, O. (2005) Binding of manganese(II) to a tertiary stabilized hammerhead ribozyme as studied by electron paramagnetic resonance spectroscopy, *RNA* 11, 1–6.
22. Morrissey, S. R., Horton, T. E., Grant, C. V., Hoogstraten, C. G., Britt, R. D., and DeRose, V. J. (1999) Mn²⁺-nitrogen interactions in RNA probed by electron spin-echo envelope modulation spectroscopy: application to the hammerhead ribozyme, *J. Am. Chem. Soc.* 121, 9215–9218.
23. Morrissey, S. R., Horton, T. E., and DeRose, V. J. (2000) Mn²⁺ sites in the hammerhead ribozyme investigated by EPR and continuous-wave q-band ENDOR spectroscopies, *J. Am. Chem. Soc.* 122, 3473–3481.
24. Qin, P. Z., Butcher, S. E., Feigon, J., and Hubbell, W. L. (2001) Quantitative analysis of the isolated GAAA tetraloop/receptor interaction in solution: a site-directed spin labeling study, *Biochemistry* 40, 6929–6936.
25. Dugas, H. (1977) Spin-labeled nucleic acids, *Acc. Chem. Res.* 10, 47–54.
26. Pscheidt, R. H., and Wells, B. D. (1986) Different conformations of the 3' termini of initiator and elongator transfer ribonucleic acids. An EPR study, *J. Biol. Chem.* 261, 7253–7256.
27. Macosko, J. C., Pio, M. S., Tinoco, I., Jr., and Shin, Y. K. (1999) A novel 5' displacement spin-labeling technique for electron paramagnetic resonance spectroscopy of RNA, *RNA* 5, 1158–1166.
28. Edwards, T. E., Okonogi, T. M., Robinson, B. H., and Sigurdsson, S. Th. (2001) Site-specific incorporation of nitroxide spin-labels into internal sites of the TAR RNA; structure-dependent dynamics of RNA by EPR spectroscopy, *J. Am. Chem. Soc.* 123, 1527–1528.
29. Edwards, T. E., Okonogi, T. M., and Sigurdsson, S. Th. (2002) Investigation of RNA-protein and RNA-metal ion interactions by electron paramagnetic resonance spectroscopy. The HIV TAR-Tat motif, *Chem. Biol.* 9, 699–706.
30. Edwards, T. E., and Sigurdsson, S. Th. (2002) Electron paramagnetic resonance dynamic signatures of TAR RNA-small molecule complexes provide insight into RNA structure and recognition, *Biochemistry* 41, 14843–14847.
31. Edwards, T. E., and Sigurdsson, S. Th. (2003) EPR spectroscopic analysis of TAR RNA-metal ion interactions, *Biochem. Biophys. Res. Commun.* 303, 721–725.
32. Qin, P. Z., Hideg, K., Feigon, J., and Hubbell, W. L. (2003) Monitoring RNA base structure and dynamics using site-directed spin labeling, *Biochemistry* 42, 6772–6783.
33. Qin, P. Z., and Dieckmann, T. (2004) Application of NMR and EPR methods to the study of RNA, *Curr. Opin. Struct. Biol.* 14, 350–359.
34. Kim, N. K., Murali, A., and DeRose, V. J. (2004) A distance ruler for RNA using EPR and site-directed spin labeling, *Chem. Biol.* 11, 939–948.
35. Edwards, T. E., Robinson, B. H., and Sigurdsson, S. Th. (2005) Identification of amino acids that promote specific and rigid TAR RNA-Tat protein complex formation, *Chem. Biol.* 12, 329–337.
36. Markley, J. C., Godde, F., and Sigurdsson, S. Th. (2001) Identification and characterization of a divalent metal ion-dependent cleavage site in the hammerhead ribozyme, *Biochemistry* 40, 13849–13856.
37. Murray, J. B., Terwey, D. P., Maloney, L., Karpeisky, A., Usman, N., Beigelman, L., and Scott, W. G. (1998) The structural basis of hammerhead ribozyme self-cleavage, *Cell* 92, 665–673.
38. Freed, J. H. (1976) Theory of slow tumbling ESR spectra for nitroxides, in *Spin labeling: Theory and application*, (Berliner, L. J., Ed.), pp 53–132, Academic Press, New York.
39. Columbus, L., and Hubbell, W. L. (2002) A new spin on protein dynamics, *Trends Biochem. Sci.* 27, 288–295.
40. Plonka, P. M., and Elas, M. (2002) Application of the electron paramagnetic resonance spectroscopy to modern biotechnology, *Curr. Top. Biophys.* 26, 175–189.
41. Hertel, K. J., Herschlag, D., and Uhlenbeck, O. C. (1994) A kinetic and thermodynamic framework for the hammerhead ribozyme reaction, *Biochemistry* 33, 3374–3385.
42. Menger, M., Tuschl, T., Eckstein, F., and Porschke, D. (1996) Mg(2+)-dependent conformational changes in the hammerhead ribozyme, *Biochemistry* 35, 14710–14716.
43. Sober, H. A., Ed. (1968) *CRC Handbook of Biochemistry: Selected data for molecular biology*, The Chemical Rubber Co., Cleveland.
44. Feig, A. L., Scott, W. G., and Uhlenbeck, O. C. (1998) Inhibition of the hammerhead ribozyme cleavage reaction by site-specific binding of Tb, *Science* 279, 81–84.
45. Feig, A. L., Panek, M., Horrocks, W. D., Jr., and Uhlenbeck, O. C. (1999) Probing the binding of Tb(III) and Eu(III) to the hammerhead ribozyme using luminescence spectroscopy, *Chem. Biol.* 6, 801–810.
46. Clouet-d'Orval, B., Stage, T. K., and Uhlenbeck, O. C. (1995) Neomycin inhibition of the hammerhead ribozyme involves ionic interactions, *Biochemistry* 34, 11186–11190.
47. Stage, T. K., Hertel, K. J., and Uhlenbeck, O. C. (1995) Inhibition of the hammerhead ribozyme by neomycin, *RNA* 1, 95–101.
48. Kirk, S. R., Luedtke, N. W., and Tor, Y. (2001) 2-Aminopurine as a real-time probe of enzymatic cleavage and inhibition of hammerhead ribozymes, *Bioorg. Med. Chem.* 9, 2295–2301.
49. Borda, E. J., and Sigurdsson, S. Th. (2004) Interactions of the antibiotics neomycin B and chlortetracycline with the hammerhead ribozyme as studied by Zn²⁺-dependent RNA cleavage, *Bioorg. Med. Chem.* 12, 1023–1028.
50. Blount, K. F., and Uhlenbeck, O. C. (2005) The Structure-Function Dilemma of the Hammerhead Ribozyme, *Annu. Rev. Biophys. Biomol. Struct.* 34, 415–440.
51. Lilley, D. M. (2003) Ribozymes—a snip too far?, *Nat. Struct. Biol.* 10, 672–673.
52. Khvorova, A., Lescoute, A., Westhof, E., and Jayasena, S. D. (2003) Sequence elements outside the hammerhead ribozyme catalytic core enable intracellular activity, *Nat. Struct. Biol.* 10, 708–712.
53. De la Pena, M., Gago, S., and Flores, R. (2003) Peripheral regions of natural hammerhead ribozymes greatly increase their self-cleavage activity, *EMBO J.* 22, 5561–5570.
54. Penedo, J. C., Wilson, T. J., Jayasena, S. D., Khvorova, A., and Lilley, D. M. (2004) Folding of the natural hammerhead ribozyme is enhanced by interaction of auxiliary elements, *RNA* 10, 880–888.
55. Menger, M., Eckstein, F., and Porschke, D. (2000) Multiple conformational states of the hammerhead ribozyme, broad time range of relaxation and topology of dynamics, *Nucleic Acids Res.* 28, 4428–4434.
56. Blount, K. F., Grover, N. L., Mokler, V., Beigelman, L., and Uhlenbeck, O. C. (2002) Steric interference modification of the hammerhead ribozyme, *Chem. Biol.* 9, 1009–1016.
57. Simorre, J. P., Legault, P., Hangar, A. B., Michiels, P., and Pardi, A. (1997) A conformational change in the catalytic core of the hammerhead ribozyme upon cleavage of an RNA substrate, *Biochemistry* 36, 518–525.
58. Murray, J. B., Szoke, H., Szoke, A., and Scott, W. G. (2000) Capture and visualization of a catalytic RNA enzyme-product complex using crystal lattice trapping and X-ray holographic reconstruction, *Mol. Cell* 5, 279–287.
59. Inoue, A., Takagi, Y., and Taira, K. (2004) Importance in catalysis of a magnesium ion with very low affinity for a hammerhead ribozyme, *Nucleic Acids Res.* 32, 4217–4223.

BI050549G